



Hydrogen evolution activity of NiMo-MoO₂ produced by mechanical milling

V. Salarvand, M. Saghafi*, M.T. Noghani

Department of Materials Science and Engineering, Faculty of Engineering, Imam Khomeini International University, Qazvin, Iran.

Received: 19 May 2019; Accepted: 1 December 2019

* Corresponding author email: msaghafi@eng.ikiu.ac.ir

ABSTRACT

In this study, mechanical alloying was done by a high-energy planetary ball milling technique. A mixture of NiO, MoO₃ and graphite powders were used as initial materials. After milling of powder mixture with 40 wt.% additional graphite, a temperature of 400, 550 and 1000 °C for 1 h was considered for the heat treatment of powder mixture. Also, powder mixtures containing 60, 80 and 100 wt.% additional graphite was heat-treated at 1000 °C for 1 h. The results of the thermodynamic analysis showed that full reduction of molybdenum-nickel oxide at ambient temperature during milling does not occur and thermal activation is required for complete reduction of mixed metal oxide. Investigation of hydrogen release through the electrochemical test in 1 M electrolyte solution of KOH at 28 °C showed that the reduced sample containing 60 wt.% additional graphite with ~187 mV additional potential in current density of ~10 mAcm⁻², has the most activity in the release of hydrogen. This sample showed the lowest R_{ct} of 17 ohm which means the good electrochemical characteristics of Ni-Mo alloy due to the good electrical conduction pathways and high access for the electrolyte solution with the high electrochemically active surface area.

Keywords: Ni-Mo alloy, Mechanical milling, Electro-chemical test, Hydrogen evolution reaction.

1. Introduction

One of the future resources, which can be used as a green, transferable, suitable and efficient fuel, is hydrogen. Hydrogen and electricity can meet energy needs and produce a form of the energy system, which is permanent and independent fuel [1]. Some hydrogen production methods can be mentioned transformation of aqueous phase to hydrogen [2], ammoniac breakout [3], biomass [4], pyrolysis [5], chemical hydrides [6], transformation of hydrocarbons to hydrogen [3] and water electrolysis [5]. Investigation of hydrogen production determines high-efficiency purity level and production costs are the main challenges of hydrogen substitution as a future energy resource.

Hydrogen can be produced in an industrial steam reforming process. A mixture of natural gas with water in low energy efficiency converts to carbon monoxide and hydrogen. The main problem with this method is the low purity of produced hydrogen due to the presence of carbon-containing residues [7]. An alternative technique for hydrogen production is water splitting with using electricity. The Advantages of this technique are the high purity of produced hydrogen and an abundance of water resources [8-12].

Furthermore, due to the zero-emission of carbon gaseous species in this technique, hydrogen is an ideal candidate for the replacement of fossil fuel energy in the future [10, 13]. In order to find

a highly efficient electro-catalyst for hydrogen production in acidic media, Pt has emerged as the most efficient one [14–15]. The main barriers of Pt for commercial application in the large scale are scarcity and high cost of this electro-catalyst. Recently, several studies try to find low-cost alternatives for Platinum. Various non-noble metal-based materials, such as transition-metal complexes [17, 18], chalcogenides [19, 20], carbide [21, 22] and metal alloys [23] were considered as catalysts or supports for the electrochemical hydrogen evolution reaction (HER).

The most active metals as hydrogen release are platinum group metals (Ir, Rh, Re, Pt), Au, Ni, Co, Fe and Cu. The determination of detailed kinetics of hydrogen production is still in progress. Meantime novel data have been provided with progress in the preparation of clean surfaces and solutions, showing much better activity in comparison with previous findings. But to achieve better results and more trustful kinetics data, more information is required. On the other hand, among the hydrogen-releasing elements, mercury has the least activity. Graphite is also semi-active but after etching in argon plasma, considerable increases in its activity was observed [24].

Obviously, beside the precious metals, none of the known methods can find the new materials among pure metals, which would possess high catalytic activity for HER. Ni-W, Ni-Mo, Ni-Co-Mo, Ni-Zn, Ni-Mo-B, Ni-Mo-Zr, Ni-Mo-Cu, Ni-Fe, Ni-Fe-Co-Mo, Ni-Mo-Fe alloys show good activity for the HER reaction [25-27]. In fact combination of two or more metals from the two branches of the “volcano” curve is suggested by Miles et. al [28]. Suggested alloys show enhanced activity for the HER and Mo-based alloys like Mo-Ni turn the main objective of the research. This alloy showed superior activity in HER with exchange current densities between 10^{-6} - 10^{-4} Acm^{-2} , compared to Pt with 10^{-3} Acm^{-2} [29].

Several researchers have done many projects on the molybdenum nickel alloy system [30-36]. Nowadays these materials are processed via diverse methods which one of them is mechanical alloying. Structure and properties of this nano material have been explored by several researchers. High activity in hydrogen release is one of the most interesting properties of this type of alloy; because the nanocrystalline state provides many active sites for the reaction [37]. Therefore production of catalysts using new procedures has attracted a great deal of

interest from many researchers. On the other hand, nickel is a non-noble and respectively cheap metal with the high electrochemical activity which is suitable for production of hydrogen electrodes used in alkaline fuel cells [38]. Also, molybdenum and its alloys are very important due to their vast catalytic activity [39, 40]. Nickel and nickel-based electrodes are one of the best materials for water electrolysis in alkaline environments due to high activity and chemical stability [41]. Nickel-molybdenum is one of the most investigated alloys produced by thermal decomposition of metallic salts and then reduction under hydrogen atmosphere. Additional potential in current density of 1000 mA/cm^2 is reported to be 83 mV for molybdenum-nickel (30-70%) [42]. Electro-catalytic properties are directly related to the size of crystals. Therefore highly-active electrodes are obtained by milling of metallic powders [30]. Through metallurgical comparison of formed phase in the diagram of Ni/Mo, it is determined that the activity of hydrogen release, increases in this manner: $\text{Ni}_4\text{Mo} < \text{Ni}_3\text{Mo} < \text{Ni}_2\text{Mo} < \text{NiMo}$ [43]. It should be mentioned that the melting point of molybdenum is $2623 \text{ }^\circ\text{C}$ and is $1455 \text{ }^\circ\text{C}$ for nickel; and also solubility limit of molybdenum in nickel is 17 wt.% at room temperature [44]. Production of nickel molybdenum with more than 17 wt.% nickel is impossible by conventional casting methods; also inter-metallic compounds in nickel-molybdenum phase diagram have the high effect on hydrogen release property [43]. Therefore the selection of a suitable and economical method is different. Production of this alloy is very important for hydrogen release. It can be produced via common thermal methods by nickel molybdenum alloys which is difficult method, so other procedures such as spark plasma [42], mechanical alloying [38], powder metallurgy [30], and electric coating [45] are used. Mechanical alloying includes particles grinding in a closed container by several metallic or ceramic balls. This method is used for processing of nanopowders, nanocomposites, oxide nanoparticles, for alloys reinforced by nanoparticles, glassy phases, intermetallic compounds and solid solutions. In fact mechanical milling is one of the methods for nano-materials processing [46, 47]. It was found that molybdenum carbide has the best activity in hydrogen liberation in comparison with molybdenum nitride and boride [48-49].

In this study, production and characterization of nickel-molybdenum nanostructure alloy have been accomplished by mechanical alloying from

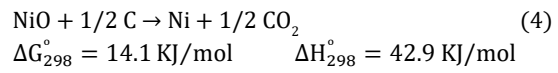
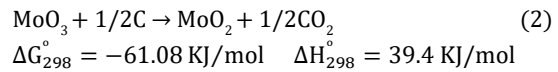
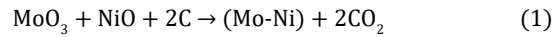
molybdenum trioxide and nickel oxide with graphite as a reducing agent, using a planetary ball mill. The aim of this research is an investigation of hydrogen release property in the produced samples. The application of oxide precursors leads to better grinding and finer particles.

2. Materials and methods

In this project, molybdenum trioxide (MoO₃ with 99.7% purity and 70 μm grain size), nickel oxide (NiO) (with a purity of 99.9% and grain size of 55 μm) and graphite (with a purity of 99.8% and a grain size less than 5 μm) were used as raw materials. Before milling, 6.99 g molybdenum trioxide, 3.62 g nickel oxide and 1.62 g graphite were scaled by a micro-balance with an accuracy of 10⁻⁴. The mixtures of molybdenum trioxide and nickel oxide were mechanically milled with 40, 60, 80 and 100 wt.% extra graphite (to complete reduction and carbide formation) in a high-energy planetary ball mill (Sanat Ceram M.A) with a container and some balls (with diameters of 9 and 14mm, hardness:68HRC) were made of hardened chromium steel for 10 h. Powder to ball ratio was 1 to 20 and the milling rate of 120 rpm were applied under argon atmosphere. Milling oxide powders in micron size lead to better grinding and finer powder particles in the nano scale. The temperature of 400, 550, 800 and 1000 °C was used for heat-treatment of the milled powder mixture. XRD technique was applied for the investigation of performed reactions. In this analysis, a copper lamp with a wavelength of 1.54 Å and an accelerator voltage of 40 kV was used in the angle range of 20 to 80 degrees. Scanning electron microscopy and also energy-dispersive X-ray spectroscopy were used for microstructural investigation and quantitative analysis of elements, respectively. Produced samples compressed into pellets with a diameter of 10 mm and 3 mm height using cold-pressing at 700 and 900 MPa. Sintering the pellets, was done in a tube furnace at 1400 °C for 1 h with a heating rate of 10 °C/min. An electrochemical experiment was required for the investigation of hydrogen release activity of produced samples. Thus a potentiostat/galvanostat device was used in a three-electrode system with a calomel electrode as a reference electrode and the platinum as a counter electrode and under conditions of 1.5 mV voltage, with a scanning rate of 10 mV/s and 1 M KOH solution at 28 °C as the electrolyte.

3. Results and discussion

In order to understand reduction procedure of powder mixture and satisfy the reaction (1), thermodynamic analysis was performed at different temperatures and it was concluded that carbothermal reduction of molybdenum trioxide occurred in two steps, which are indicated in reactions (2) and (3); also carbothermal reduction of nickel oxide as indicated in equation (4).



Variations of the free energy of each reaction are indicated in figure 1. Results of this investigation showed that for the accomplishment of molybdenum trioxide and nickel oxide reaction a thermodynamic derivative force existed due to the negativity of ΔG (ΔG₂₉₈^o = -61.08KJ/mol). Therefore high probability of reaction (2) via milling was thermodynamically predictable. A thermodynamic barrier is as big as 137.7 KJ/mol. existed at room temperature which mechanical milling could not overcome. According to figure 1 the size of the barrier reduced at higher temperatures (around 1000 K). This temperature was much higher than the milling temperature. Regarding the performed investigations, two ways could be used for the reduction of oxide mixture; one the milling at high

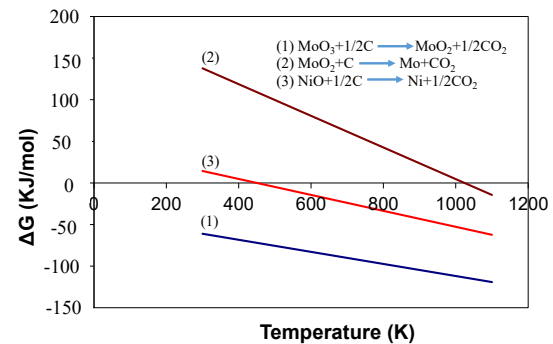


Fig. 1- Thermodynamic analysis of reactions related to the powder mixture.

temperatures and the second performing heat-treatment at high temperatures for room milled sample that second procedure selected in this research.

Regarding the obtained results from DTA/TG analysis indicated in figure 2 and confirmed by thermodynamic analysis, the temperature of heat-treatment was selected below 1000 °C so that reduction of each oxide precursor was visible in X-ray diffraction analysis. No reaction occurred in the mixture heat-treated below 400 °C; and with increasing the temperature, a descending slope was observed in the thermal differential decomposition diagram escorted by some weight loss. Regarding thermodynamic analysis, the reduction of nickel oxide had occurred. Therefore the temperature of 550 °C was selected for heat-treatment. Below 800 °C, a downfall has appeared which was along with an extreme weight loss. The reaction between existing oxygen in oxide powders and graphite which led to the formation of CO₂ gas was mentioned as weight loss reason. So the temperature of 800 °C was selected for heat-treatment. The reduction temperature of molybdenum oxide can be decreased by milling of the powder mixture and also the addition of surplus graphite to the stoichiometric compound. So the temperature of 1000 °C was considered for heat-treatment to investigate the reduction of molybdenum oxide.

X-ray diffraction results of oxide powders and milled powder mixtures for 10 min, 10 h and, 30 h were investigated and shown in figure 3. In the sample which was only milled for 10 min, graphite peak was observed along with nickel oxide and molybdenum trioxide peaks, but graphite peak

disappeared after 10 h of milling time and a decrease in the intensity of oxide powder peaks was also observed. Milling for 30 h did not lead to the reduction of oxide powders but resulted in a decrease in the oxide peaks intensities. It is worth to note that as there was a big barrier to molybdenum reduction process from the thermodynamic investigation. Milling more than 200 h did not occur any reduction but it helped MoO₃ to reduce into MoO₂ [50].

X-ray diffraction results of the sample containing 40 wt.% additional graphite at temperatures of 400, 550 and 800 °C was shown in figure 4. As it was expected no reaction below 400 °C heat-treatment has occurred. As it was expected heat-treatment at 550 °C led to the transformation of MoO₃ to MoO₂; but NiO left it in the structure without any changes. Regarding thermodynamic predictions, differential thermal analysis and lack of reduction of nickel oxide at 550 °C is concluded that reduction occurred in the temperature range of 550-600 °C.

Reduction of NiO and partial reaction MoO₂ (existing in the structure) with graphite led to the formation of a complex structure of Ni₆Mo₆C_{1/06} observed in the X-ray diffraction pattern of the heat-treated sample at 800 °C.

To obtain nickel-molybdenum alloy, the powder mixture with different percentages of additional graphite was heat-treated at 1000 °C. As it is observed in the X-ray diffraction pattern (figure 5), the reduced sample with 40 wt.% additional graphite had the structure of nickel-molybdenum alloy with some MoO₂ in the structure. This sample was considered as nickel-molybdenum alloy along with some molybdenum oxide. To reduce MoO₂ amount in the structure, 60 wt.% additional

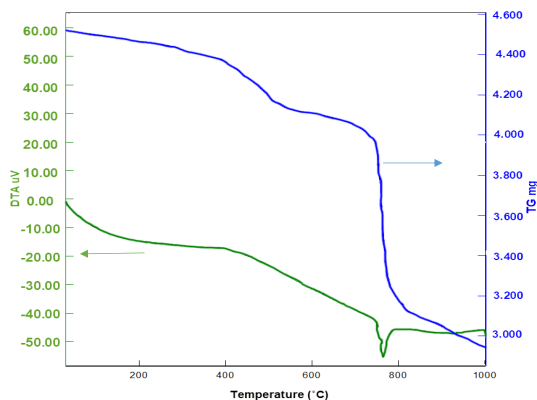


Fig. 2- Differential thermal analysis of powder mixture with 40 wt.% extra graphite, milled for 10h.

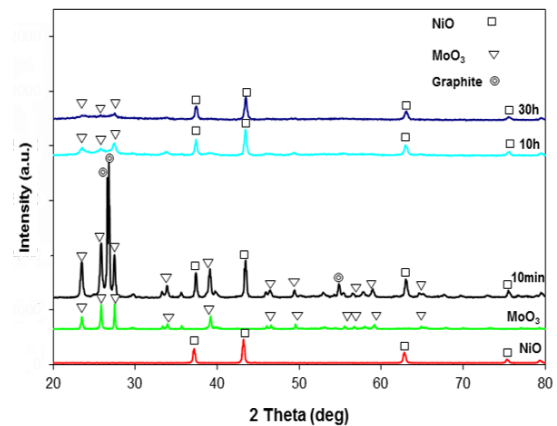


Fig. 3- X-ray patterns of 40 wt.% extra graphite milled sample with different milling durations.

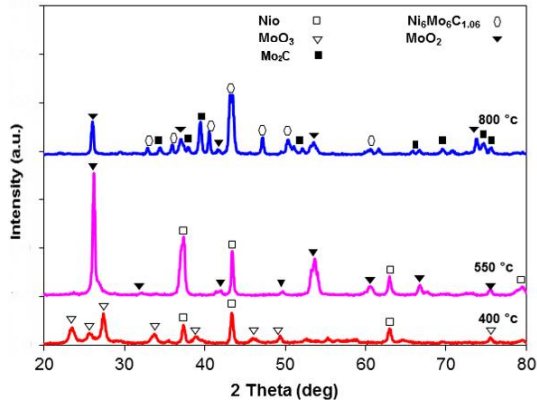


Fig. 4- X-ray diffraction pattern of the sample containing 40 wt.% extra graphite and heat-treated at different temperatures.

graphite was used which led to the production of nickel-molybdenum with molybdenum oxide which the amount of MoO₂ in this sample is less than the previous reduced sample with 40 wt.% additional graphite. This sample was selected as the nickel-molybdenum alloy. The presence of some MoO₂ in the structure could be resulted from two reasons: 1) the used argon gas had not been pure completely and 2) over-adhesion of graphite to the tubes or milling container had inhibited complete reduction of oxide powders. Of course a low amount of MoO₂ in the structure was negligible and on the other hand, its effect on hydrogen release activity could be investigated. Figure 5 shows that the reduced sample containing 80 wt.% additional graphite includes Ni₅Mo₆C and Mo₂C phases and also nickel-molybdenum alloy. To increase the amount of Mo₂C and its effect on hydrogen release activity, 100 wt.% extra graphite during milling was used; but no significant difference in structure compared with the reduced sample containing 80 wt.% extra graphite was observed. However, the amount of Mo₂C was increased in the sample. The crystallite size of Mo-Ni during ball milling can be determined from broadening of XRD peaks by Scherer equation:

$$D = k\lambda / \beta \cos\theta \quad (\text{eq. 1})$$

Where D is the grain size, λ is the X-ray wavelength, β is the line width at one-half the maximum intensity and θ is the Bragg angle (in degrees). The crystallite size of molybdenum-nickel reduced with 40 wt% extra graphite was measured to be 52 nm.

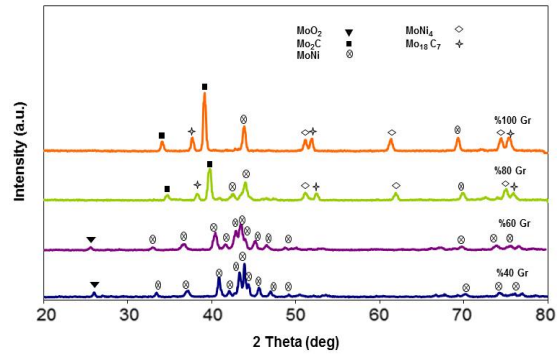


Fig. 5- X-ray diffraction patterns of heat treated powder mixture with different percentages of additional graphite reduced at 1000 °C.

After the production of desired samples, grain size and their microstructure were investigated by scanning electron microscopy. It was clarified that the production of the alloy was accomplished in the nano-scale. Application of oxide materials had a significant effect on particle size, shifting them to a smaller scale due to the acceleration of grinding rate respective to the re-sintering rate of them. Also, elemental spectroscopy was used to investigate the existing elements in the structure. Regarding this fact that some oxygen and carbon were left in the structure after production of nickel-molybdenum alloy via reduction of oxide powders. The presence of these two elements had a significant effect on hydrogen release activity of nickel-molybdenum alloy.

Figure 6 shows images of scanning electron microscopy and elemental spectroscopy analysis of reduced samples containing 40 wt.% (Fig. 6a and b), 60 wt.% (Fig. 6c and d), 80 wt.% (Fig. 6e and f), and 100 wt.% (Fig. 6g and h) extra graphite additive after milling for 10 h and heat-treated at 1000 °C for 1 h. the mean particle size of all samples was measured to be 86.2, 75.9, 96.5, 86.5 100 nm respectively. Also, the shape of particles reduced with 40, 60 and 100 wt.% extra graphite additive was irregular, while the shape of particle for 80 wt.% graphite additive was spherical-irregular. According to X-ray diffraction results, the reduced sample with 40 wt.% extra graphite additive contained nickel-molybdenum alloy and some percentage MoO₂. Spectroscopy of this sample shows that the oxygen and carbon contents were 12.66 and 5.33 wt.% respectively. The presence of molybdenum oxide in the phase analysis of this sample confirmed the above-mentioned results.

X-ray diffraction results of the reduced sample with 60 wt.% extra graphite additive; confirmed that the sample contained nickel-molybdenum alloy and a percentage of MoO_2 . Spectroscopy of this sample indicated that the oxygen amount was reduced in this sample and reached 6.23 wt.%. This is proof of a better reaction between free carbon and oxygen in the structure and formation of CO_2 .

According to the X-ray diffraction pattern of the reduced sample with 80 wt.% extra graphite additive, this sample contained nickel-molybdenum alloy, MoNi_4 and Mo_{18}C_7 intermetallic compounds. Elemental spectroscopy analysis of this sample

indicated that the oxygen level was reached to 3.13 wt.%. As it was observed in the investigation of X-ray diffraction, oxide structure was not found due to the complete reaction of existing oxygen in the structure with carbon. According to the X-ray diffraction pattern of reduced sample with 100 wt.% extra graphite additive, this sample contained nickel-molybdenum alloy, Mo_2C , MoNi_4 and Mo_{18}C_7 intermetallic compounds. Also, elemental spectroscopy analysis showed that no significant difference has existed between structures of the reduced sample containing 100 wt.% and 80 wt.% additional graphite. However, the amount of carbon

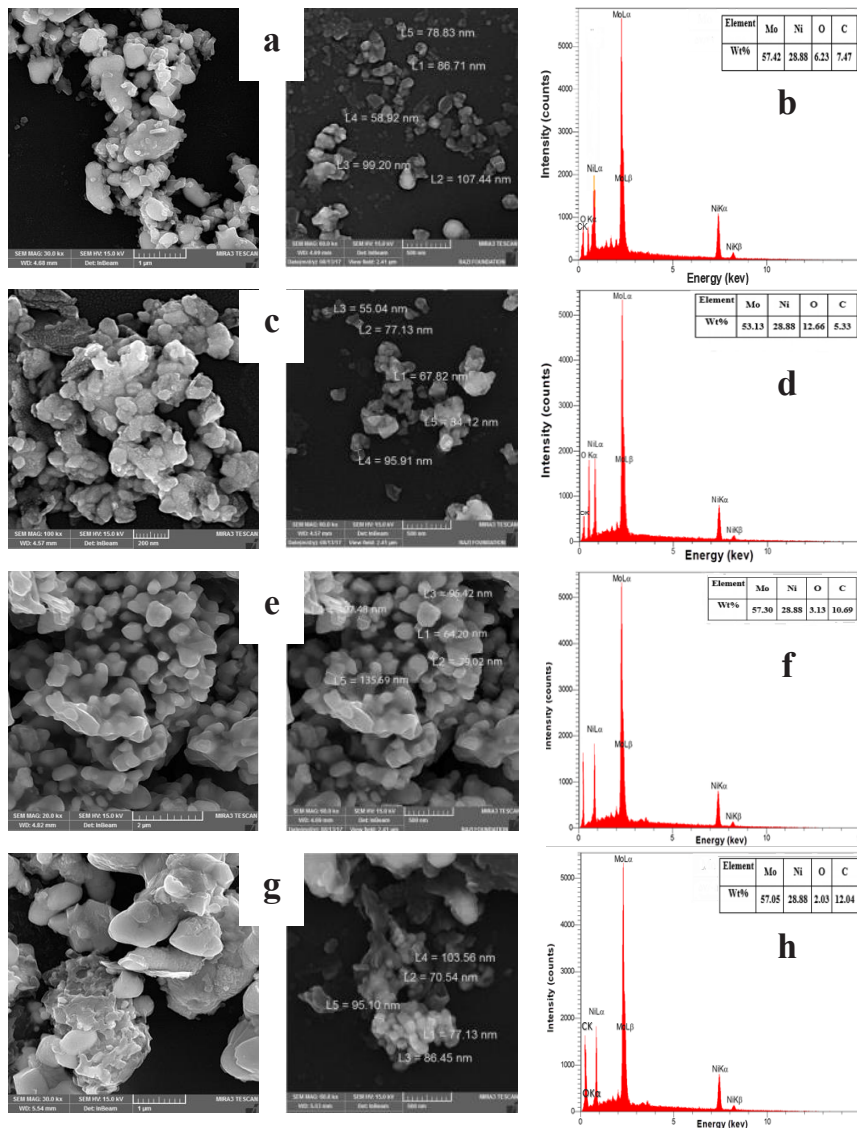


Fig. 6- SEM images and EDS analysis of various electrodes with different percentages of additional graphite. (a, b) 40 wt.%, (c, d) 60 wt.%, (e, f) 80 wt.%, (g, h) 100 wt.%.

increased in this sample and reached 12.04 wt.%. Table 1 shows the hardness of samples pressed at 700 MPa and sintered at 1400 °C. The results show that the consolidation condition could be suitable for the sample using as HER electro catalyst.

After phase analysis and structural investigations, produced samples were pressed at 700 and 900 MPa and sintered at 1400 °C. The cold press was used for stabilization of samples while hot press led to the addition of oxygen to the structure and formation of molybdenum oxide. Also, hot press led to the formation of intermetallic compounds in the structure [49]. The cathodic linear polarization graph of samples is observed in figure 7 which using the hydrogen release activity of different samples was investigated. In this diagram the current density of 10 mA/cm² was considered. According to table 2 voltage of reduced sample with 40 wt.% additional graphite pressed at 700 MPa in the considered current was 200 mV which had lower activity in the release of hydrogen compared with the reduced sample containing 60 wt.% additional graphite and which had a voltage of 187 mV. Regarding the fact that the presence of MoO₂ in nickel-molybdenum alloy had a positive

effect on increasing the hydrogen release activity [49]; but it seemed that the amount of this material in the structure of nickel-molybdenum alloy had an optimum limit. This was the reason for lower activity observed in the reduced sample with 40 wt.% additional graphite which had a higher amount of MoO₂. On the other hand, as the presence of 1 wt.% oxygen in the structure led to the activation of alloy and improvement of hydrogen release activity in nickel-molybdenum alloy [51]. Investigation of carbide samples (Mo₂C had respectively good activity in hydrogen release) was expected that the reduced sample containing 100 wt.% extra graphite with a higher amount of Mo₂C compared with the reduced sample containing 80 wt.% extra graphite had a higher activity which confirmed at table 2. No significant difference was observed in the release activity of these two samples, and the reason for little inequality was the same percentages of Mo₂C in their structure. Further comparisons of HER activity between all electrodes and commercial available Pt/20%C catalyst were also performed. As presented in figure 7, Pt/20%C catalyst exhibits extremely high HER catalytic activity with a near zero onset potential and large current density at the

Table 1- The hardness of samples pressed at 700 MPa and sintered at 1400 °C

Sample	Hardness (Hv)
reduced sample with 40 wt.% extra graphite	612
reduced sample with 60 wt.% extra graphite	734
reduced sample with 80 wt.% extra graphite	519
reduced sample with 100 wt.% extra graphite	649

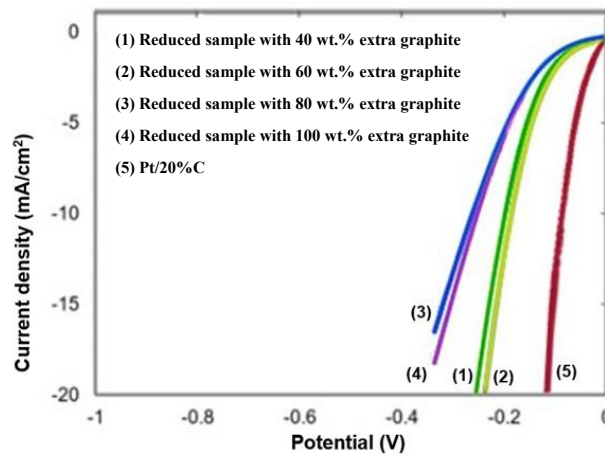


Fig. 7- Polarization curves of various electrodes recorded during cathodic polarization in 1 M KOH at the scan rate of 10 mV s⁻¹.

same over potential. Reduced sample with 40 wt.% additional graphite shows the best activity and near behavior to Pt/20%C catalyst. The samples prepared at 900 MPa pressure showed higher current density in which means higher activity as compared to the pressed sample at 700 MPa. In fact with using higher pressure for the consolidation of powder samples, the active surface area could be increased [52].

The electro-catalytic performance of the samples in the hydrogen evolution reaction from 1 M KOH solution at 28°C was investigated by electrochemical impedance spectroscopy technique. The Nyquist curves and the equivalent electrical circuit is shown in figure 8. In this circuit, the solvent resistance is shown with R_s , which $CPE1$ represents the dual layer capacity and C_p is the false capacitive capacity. Also, R_f represents the absorption resistance of hydrogen at the electrode surface, and R_{ct} represents the electrochemical charge transfer resistance. As shown in Table 3, in

the reduced sample with 60 wt.% excess carbon, the charge transfer resistance has reached the lowest value of 17 Ω. It should be noted that for this observed decrease of charge transfer resistance parameter in the produced samples is in accordance with the increase in current density obtained by polarization analysis measurements.

To compare the results of this study with other papers, the hydrogen evolution activity of the sample with 60% excess graphite was compared with the activity of different materials and the results has shown in Table 4. In the sample of this study, at the Tafel slope of 75 mv/dec and the additional potential in the current density of 10 mA/cm², the activity of hydrogen evolution is 187 mV. In the case of a commercial sample of Pt/20 wt% C, the conditions are much better in such a way that the additional potential is 30 mV at a current density of -10 mA/cm². The electrode has now been commercialized, but due to the high cost of platinum, extensive researches have done to

Table 2- Kinetics parameters from hydrogen release reaction obtained from polarization linear curve and Tafel curve in 1 M KOH electrolyte at 28 °C

Sample	pressure	bc (mVdec ⁻¹)	η (10 mAcm ⁻²)	j^0 (mAcm ⁻²)
reduced sample with 40 wt.% extra graphite	700	75	-200	0.255
	900	81		0.338
reduced sample with 60 wt.% extra graphite	700	71	-187	0.289
	900	78		0.425
reduced sample with 80 wt.% extra graphite	700	130	-263	0.163
	900	122		0.202
reduced sample with 100 wt.% extra graphite	700	126	-251	0.201
	900	119		0.253
Pt %20C	-	30	-40	0.39

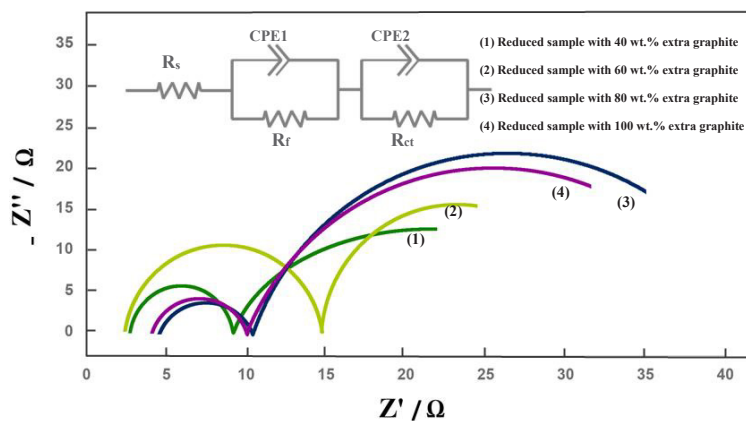


Fig. 8- Nyquist plots of various electrodes in 1 M KOH.

Table 3- EIS fitting parameters of Ni-Mo electrodes pressed at 700 MPa

Parameters	reduced sample with 40 wt.% extra graphite		reduced sample with 60 wt.% extra graphite		reduced sample with 80 wt.% extra graphite		reduced sample with 100 wt.% extra graphite	
	Value	Error (%)	Value	Error (%)	Value	Error (%)	Value	Error (%)
$R_s (\Omega)$	2.3	4.2	2.1	2	4.8	2.3	4.5	3.3
$C_p (\mu F)$	0.91	1.8	0.97	3.2	0.91	2.5	0.91	2.4
$C_{dl} (\mu F)$	0.0018	3.3	0.003	1.4	0.0008	3.1	0.0008	4.55
$R_f (\Omega)$	6.6	11.2	12.7	4.7	5.6	1.7	5.5	1.4
$C_p (\mu F)$	0.83	2.3	1.09	2.6	0.69	4.2	0.8	2
$C_{dl} (\mu F)$	0.97	2.6	1.129	2.8	0.87	0.8	0.91	3.9
$R_{ct} (\Omega)$	25	2.1	17	3.1	35	2.6	32	5.3

Table 4- Comparison of different materials activity with the sample reduced with 60% of excess

Activity	electrolyte	Tafel slope (mV/decade)	activity	Ref
sample with 60% excess graphite	1 M KOH	71	$\eta_{-10} = -187\text{mV}$	This work
20 wt%Pt/C	1 M NaOH	31	$\eta_{-10} = -30\text{mV}$	[53]
$\text{Ni}_{72}\text{Co}_{28}$	1 M NaOH	64	$\eta_{-10} = -198\text{mV}$	[53]
Ni	1 M NaOH	68	$\eta_{-10} = -221\text{mV}$	[53]
$\text{Ni}_{70}\text{Mo}_{28}\text{Cu}_2$	6 M KOH	144	$\eta_{-10} = -308\text{mV}$	[53]
NiMo(66.2/33.88%)	30% KOH	185	$\eta_{-100} = -262\text{mV}$	[54]
Ni60Mo40	30% KOH	107	$\eta_{250} = 404\text{mV}$	[29]

replace another material that has high activity and economic value. In the case of the $\text{Ni}_{72}\text{Co}_{28}$ sample, given the amount of potential in the same current density, it can be stated that this sample has lower activity than the sample of our study. In the cases of Ni, $\text{Ni}_{70}\text{Mo}_{28}\text{Cu}_2$, Ni-Mo(66.2-33.88%) and Ni60Mo40, also the hydrogen evolution activity is lower than the activity of this study. Here, in addition to being confirmed that the alloying has increased the hydrogen evolution activity in most materials, it can be seen that mechanical alloying increases the activity of hydrogen evolution in the molybdenum-nickel alloy as opposed of synthesizing by melting method. Also, the effect of MoO_2 along with molybdenum-nickel alloy in hydrogen evolution with elements such as copper and cobalt can be investigated [53, 54].

4. Conclusion

Adding different percentages of excess graphite to the stoichiometric composition of the MoO_3 and NiO powders mixture after heat treatment at 1000 °C, the samples were produced in addition to molybdenum-nickel alloy with some Mo_2C and MoO_2 as an impurity. For this reason, it was

possible to investigate the effect of Mo_2C and MoO_2 on the electro-catalytic activity of molybdenum-nickel alloy, which the reduced sample with 60 wt.% excess graphite with a Tafel slope of 71 mV/dec, current density of 0.289 mV/cm² and resistance to charge transfer of 17 Ω has the highest activity in hydrogen evolution reaction.

5. Acknowledgments

The financial support of this work by the Research Council of Imam Khomeini International

References

1. Sherif SA, Barbir F, Veziroglu TN. Wind energy and the hydrogen economy—review of the technology. *Solar Energy*. 2005;78(5):647-60.
2. Wen G, Xu Y, Ma H, Xu Z, Tian Z. Production of hydrogen by aqueous-phase reforming of glycerol. *International Journal of Hydrogen Energy*. 2008;33(22):6657-66.
3. Palo DR, Dagle RA, Holladay JD. Methanol Steam Reforming for Hydrogen Production. *Chemical Reviews*. 2007;107(10):3992-4021.
4. Levin DB, Zhu H, Beland M, Cicek N, Holbein BE. Potential for hydrogen and methane production from biomass residues in Canada. *Bioresource Technology*. 2007;98(3):654-60.
5. Muradov N. Emission-free fuel reformers for mobile and portable fuel cell applications. *Journal of Power Sources*. 2003;118(1-2):320-4.

6. Amendola SC, Sharp-Goldman SL, Janjua MS, Kelly MT, Petillo PJ, Binder M. An ultrasafe hydrogen generator: aqueous, alkaline borohydride solutions and Ru catalyst. *Journal of Power Sources*. 2000;85(2):186-9.
7. Häussinger P, Lohmüller R, Watson AM. Hydrogen, 2. Production. *Ullmann's Encyclopedia of Industrial Chemistry*, 2000.
8. Liang Y, Li Y, Wang H, Dai H. Strongly Coupled Inorganic/Nanocarbon Hybrid Materials for Advanced Electrocatalysis. *Journal of the American Chemical Society*. 2013;135(6):2013-36.
9. Wang H, Dai H. Strongly coupled inorganic-nano-carbon hybrid materials for energy storage. *Chemical Society Reviews*. 2013;42(7):3088.
10. Dresselhaus MS, Thomas IL. Alternative energy technologies. *Nature*. 2001;414(6861):332-7.
11. Carmo M, Fritz DL, Mergel J, Stolten D. A comprehensive review on PEM water electrolysis. *International Journal of Hydrogen Energy*. 2013;38(12):4901-34.
12. Zeng K, Zhang D. Recent progress in alkaline water electrolysis for hydrogen production and applications. *Progress in Energy and Combustion Science*. 2010;36(3):307-26.
13. Turner JA. Sustainable Hydrogen Production. *Science*. 2004;305(5686):972-4.
14. Chen W-F, Sasaki K, Ma C, Frenkel AI, Marinkovic N, Muckerman JT, et al. Hydrogen-Evolution Catalysts Based on Non-Noble Metal Nickel-Molybdenum Nitride Nanosheets. *Angewandte Chemie International Edition*. 2012;51(25):6131-5.
15. Antolini E. Platinum-based ternary catalysts for low temperature fuel cells. *Applied Catalysis B: Environmental*. 2007;74(3-4):324-36.
16. Serov A, Kwak C. Review of non-platinum anode catalysts for DMFC and PEMFC application. *Applied Catalysis B: Environmental*. 2009;90(3-4):313-20.
17. Evans DJ, Pickett CJ. Chemistry and the hydrogenases. *Chemical Society Reviews*. 2003;32(5):268.
18. Volbeda A, Fontecilla-Camps JC. The active site and catalytic mechanism of NiFe hydrogenases. *Dalton Trans*. 2003(21):4030-8.
19. Hinnemann B, Moses PG, Bonde J, Joergensen KP, Nielsen JH, Horch S, et al. Biomimetic Hydrogen Evolution: MoS₂ Nanoparticles as Catalyst for Hydrogen Evolution. *ChemInform*. 2005;36(25).
20. Wu Z, Fang B, Bonakdarpour A, Sun A, Wilkinson DP, Wang D. WS₂ nanosheets as a highly efficient electrocatalyst for hydrogen evolution reaction. *Applied Catalysis B: Environmental*. 2012;125:59-66.
21. Vrabel H, Hu X. Molybdenum Boride and Carbide Catalyze Hydrogen Evolution in both Acidic and Basic Solutions. *Angewandte Chemie*. 2012;124(51):12875-8.
22. Harnisch F, Schröder U, Quaaas M, Scholz F. Electrocatalytic and corrosion behaviour of tungsten carbide in near-neutral pH electrolytes. *Applied Catalysis B: Environmental*. 2009;87(1-2):63-9.
23. McKone JR, Sadtler BF, Werlang CA, Lewis NS, Gray HB. Ni-Mo Nanopowders for Efficient Electrochemical Hydrogen Evolution. *ACS Catalysis*. 2013;3(2):166-9.
24. Dabo P, Brossard L, Me Nard H, Tremblay P. *Journal of Applied Electrochemistry*. 1998;28(6):601-6.
25. Li N, Huang JM, Chen WZ, Wang B. Electrochemical Characteristics of the Amorphous-Nanocrystal Ni-Mo Cathodes in Sodium Hydroxide Solution. *Key Engineering Materials*. 2015;667:280-5.
26. Luo B, Ren B, Xu Y, Zheng Y. A new method to improve surface morphology of Ni-Fe-Mo-Co alloy electrode and its catalytic activity for HER. *Rare Metals*. 2007;26(3):205-12.
27. Arulraj I. Nickel based composite electrolytic surface coatings as electrocatalysts for the cathodes in the energy efficient industrial production of hydrogen from alkaline water electrolytic cells. *International Journal of Hydrogen Energy*. 1992;17(6):413-21.
28. Miles MH. Evaluation of electrocatalysts for water electrolysis in alkaline solutions. *Journal of Electroanalytical Chemistry and Interfacial Electrochemistry*. 1975;60(1):89-96.
29. Huot JY. Low Hydrogen Overpotential Nanocrystalline Ni-Mo Cathodes for Alkaline Water Electrolysis. *Journal of The Electrochemical Society*. 1991;138(5):1316.
30. Divisek J, Schmitz H, Balej J. Ni and Mo coatings as hydrogen cathodes. *Journal of Applied Electrochemistry*. 1989;19(4):519-30.
31. Tawancy HM. Comparative corrosion behavior of Ni-Mo and Ni-Mo-Cr alloy for applications in reducing environments. *Journal of Materials Science*. 2006;41(24):8359-62.
32. Chen L. Hydrogen Evolution Reaction on Nickel-Molybdenum Powder Electrodes. *Journal of The Electrochemical Society*. 1992;139(12):3458.
33. McKay IS, Schwalbe JA, Goodman ED, Willis JJ, Majumdar A, Cargnello M. Elucidating the synergistic mechanism of nickel-molybdenum electrocatalysts for the hydrogen evolution reaction. *MRS Communications*. 2016;6(3):241-6.
34. McKone JR, Sadtler BF, Werlang CA, Lewis NS, Gray HB. Ni-Mo nanopowders for efficient electrochemical hydrogen evolution. *ACS catalysis*. 2013;3(2):166-9.
35. Ahmad YH, Mohamed AMA, Golden TD, and D'Souza N. Electrodeposition of nanocrystalline Ni-Mo alloys from alkaline glycinate solutions. *International Journal of Electrochemical Science*. 2014;9:6438-50.
36. Zhang L, Xiong K, Nie Y, Wang X, Liao J, Wei Z. Sputtering nickel-molybdenum nanorods as an excellent hydrogen evolution reaction catalyst. *Journal of Power Sources*. 2015;297:413-8.
37. Kedzierzawski P, Oleszak D, Janik-Czachor M. Hydrogen evolution on hot and cold consolidated Ni-Mo alloys produced by mechanical alloying. *Materials Science and Engineering: A*. 2001;300(1-2):105-12.
38. Kenjo T. Chromium-Doped Raney Nickel Catalyst for Hydrogen Electrodes in Alkaline Fuel Cells. *Journal of The Electrochemical Society*. 1985;132(2):383.
39. Abdel-Karim R, Halim J, El-Raghy S, Nabil M, Waheed A. Surface morphology and electrochemical characterization of electrodeposited Ni-Mo nanocomposites as cathodes for hydrogen evolution. *Journal of Alloys and Compounds*. 2012;530:85-90.
40. Beltowska-Lehman E, Indyka P. Kinetics of Ni-Mo electrodeposition from Ni-rich citrate baths. *Thin Solid Films*. 2012;520(6):2046-51.
41. Kibria M. Electrochemical studies of a nickel electrode for the hydrogen evolution reaction. *International Journal of Hydrogen Energy*. 1995;20(6):435-40.
42. Brown DE, Mahmood MN, Man MCM, Turner AK. Preparation and characterization of low overvoltage transition metal alloy electrocatalysts for hydrogen evolution in alkaline solutions. *Electrochimica Acta*. 1984;29(11):1551-6.
43. Jakšić JM, Vojnović MV, Krstajić NV. Kinetic analysis of hydrogen evolution at Ni-Mo alloy electrodes. *Electrochimica Acta*. 2000;45(25-26):4151-8.
44. Gennero de Chialvo MR, Chialvo AC. Hydrogen evolution reaction on smooth Ni(1-x)+Mo(x) alloys (0≤x≤0.25). *Journal of Electroanalytical Chemistry*. 1998;448(1):87-93.

45. Raj IA, Vasu KI. Transition metal-based hydrogen electrodes in alkaline solution ? electrocatalysis on nickel based binary alloy coatings. *Journal of Applied Electrochemistry*. 1990;20(1):32-8.
46. Suryanarayana C, Ivanov E, Boldyrev VV. The science and technology of mechanical alloying. *Materials Science and Engineering: A*. 2001;304-306:151-8.
47. Anantharaman TR, Suryanarayana C. Review: A decade of quenching from the melt. *Journal of Materials Science*. 1971;6(8):1111-35.
48. Regmi YN, Waetzig GR, Duffee KD, Schmuecker SM, Thode JM, Leonard BM. Carbides of group IVA, VA and VIA transition metals as alternative HER and ORR catalysts and support materials. *Journal of Materials Chemistry A*. 2015;3(18):10085-91.
49. Ma L, Ting LRL, Molinari V, Giordano C, Yeo BS. Efficient hydrogen evolution reaction catalyzed by molybdenum carbide and molybdenum nitride nanocatalysts synthesized via the urea glass route. *Journal of Materials Chemistry A*. 2015;3(16):8361-8.
50. Saghafi M, Ataie A, Heshmati-Manesh S. SOLID STATE REDUCTION OF MoO₃ WITH CARBON VIA MECHANICAL ALLOYING TO SYNTHESIZE NANO-CRYSTALLINE MoO₂. *International Journal of Modern Physics: Conference Series*. 2012;05:441-7.
51. Schulz R, Huot JY, Trudeau ML, Dignard-Bailey L, Yan ZH, Jin S, et al. Nanocrystalline Ni-Mo alloys and their application in electrocatalysis. *Journal of Materials Research*. 1994;9(11):2998-3008.
52. Rodríguez-Valdez L. Electrochemical performance of hydrogen evolution reaction of Ni-Mo electrodes obtained by mechanical alloying. *International Journal of Hydrogen Energy*. 2004.
53. Sun T, Cao J, Dong J, Du H, Zhang H, Chen J, et al. Ordered mesoporous Ni Co alloys for highly efficient electrocatalytic hydrogen evolution reaction. *International Journal of Hydrogen Energy*. 2017;42(10):6637-45.
54. Huang L, Yang F-z, Xu S-k, Zhou S-m. Studies of Structure and Electrocatalytic Hydrogen Evolution on Electrodeposited Nanocrystalline Ni-Mo Alloy Electrodes. *Transactions of the IMF*. 2001;79(4):136-9.